Chinese Chemical Letters 34 (2023) 107321

Contents lists available at ScienceDirect

Chinese Chemical Letters

journal homepage: www.elsevier.com/locate/cclet

Single-bond-linked oligomeric donors for high performance organic solar cells

Min Lv[a,b], Yi Tang[a,b], Dingding Qiu[a,b], Wenjun Zou[a,*], Ruimin Zhou[a,b], Lixuan Liu[a,b], Ziyun Huang[a,b], Jianqi Zhang[a], Kun Lu[a,b,*], Zhixiang Wei[a,b]

[a] CAS Key Laboratory of Nanosystem and Hierarchical Fabrication, CAS Center for Excellence in Nanoscience, National Center for Nanoscience and Technology, Beijing 100190, China
[b] University of Chinese Academy of Sciences, Beijing 100049, China

ARTICLE INFO

Article history:
Received 23 November 2021
Revised 13 December 2021
Accepted 10 March 2022
Available online 13 March 2022

Keywords:
Linked donor
Oligomeric donors
Molecular stacking orientation
Organic solar cells

ABSTRACT

The effective design and synthesis of novel small-molecule donors (SMDs) is extremely essential for the in-depth study of the scientific problems of bulk heterojunction morphology and the improvement of photovoltaic performance in organic solar cells (OSCs). Importantly, developing a series of donors with different conjugated central donor (D) units is a remarkable strategy to obtain high-performance donors. Herein, two acceptor-donor-donor-acceptor (A-D-D-A) type oligomeric donors 2DTBDT and 2DTBDT-2T with two dithieno[2,3-*d*:2′,3′-*d*']benzo[1,2-*b*:4,5-*b*']dithiophene (DTBDT) as D units, without and with bithiophene as the π bridge respectively are designed and synthesized successfully. The central linked-DTBDT unit can provide a larger conjugated plane and promote π electron delocalization, which can effectively improve π-π interactions between donors and regulate the crystallinity. And we found that the π bridge provided 2DTBDT-2T with 12.31% efficiency that is already a high efficiency in OSCs, whereas 2DTBDT with merely 3.63% efficiency, both with 2,2′-((2*Z*,2′*Z*)-((12,13-bis(2-ethylhexyl)-3,9-diundecyl-12,13-dihydro-[1,2,5]thiadiazolo[3,4-*e*]thieno[2,"3'':4′,5′]thieno[2′,3′:4,5]pyrrolo[3,2-*g*]thieno-[2′,3′:4,5]thieno[3,2-*b*]indole,10-diyl)bis(methanylylidene))bis(5,6-difluoro-3-oxo-2,3-dihydro-1*H*-indene-2,1-diylidene)) dimalononitrile (Y6) as the acceptor. We conjecture that the main reason for the different device performance may be ascribed to the different molecular stacking orientation of the oligomeric donors and morphology features of the donors:Y6 blend films. Compared to the predominant face-on orientation of the 2DTBDT neat film, the 2DTBDT-2T neat film performed a preferential edge-on orientation, which obtained a smoother surface, stronger crystallinity and more uniform phase separation in the 2DTBDT-2T:Y6 blend films with nanofiber structure, which delivered higher and more balanced carrier mobilities, the more efficient exciton dissociation and reduced biomolecule recombination, therefore obtaining better power conversion efficiencies (PCEs). We speculate that the transformation of molecular stacking orientation of oligomeric donors is possibly due to that π bridge extended and twisted the molecular structure of 2DTDBT-2T, resulting in an edge-on orientation relative to the substrate. These findings demonstrate that the single-bond-linked donor strategy is an alternative method to design the donors towards high-performance OSCs.

The solution-processed bulk heterojunction (BHJ) organic solar cells (OSCs) are considered the effective devices for converting renewable clean light energy into electricity due to their advantages of light weight, flexibility, compatibility with large-area fabrication and semi-transparency, which have received extensive academic and commercial attention [1–10]. In general, BHJ-OSCs are mainly divided into polymer solar cells (PSCs), all-polymer cells and all-small-molecule organic solar cells (ASM-OSCs). Driven by the development of new materials, including non-fullerene acceptors (NFAs), polymer acceptors, polymer donors and small-molecule donors [11–14], the power conversion efficiencies (PCEs) of OSCs have increased substantially in the past few years. Currently, a significant breakthrough in PCEs that has approached 19% achieved in OSCs by combining material design with a ternary blending strategy reported by Hou's group [15]. At the same time, benefiting from the advantages of NFAs and small molecular donors (SMDs) with well-defined structures, less batch-to-batch variation and versatile chemical structures, the PCE of ASM-OSCs has been con-

* Corresponding authors.
E-mail addresses: zouwj@nanoctr.cn (W. Zou), lvk@nanoctr.cn (K. Lu).

https://doi.org/10.1016/j.cclet.2022.03.044
1001-8417/

tinuously refreshed and successfully upgraded to more than 17% [16]. However, in consequence of inappropriate crystallinity and unmanageable nano-scale bi-continuous interpenetrating networks in blend films resulting from similar and shorter acceptor-donor-acceptor (A-D-A) structures and inefficient pre-aggregation properties between SMDs and NFAs, the PCEs of current state-of-the-art ASM-OSCs are still much lower than that of polymer-based OSCs. Therefore, the exploitation of novel SMDs with better photovoltaic performance matching to the acceptors is particularly important to further improve the PCEs and study the scientific issues of OSCs systems in depth [17–21].

Importantly, adjusting the crystallinity and molecular stacking orientation of SMDs by structural design is an effective measure to obtain a blend film with excellent morphology in ASM-OSCs. Previous studies have shown that increasing the conjugated structure of molecules to regulate the crystallinity of SMDs can make the blend films have a more suitable phase separation morphology for exciton dissociation and transport, thus achieving considerable photovoltaic performance [22–36]. Among the available SMDs, benzo[1,2-*b*:4,5-*b*']dithiophene (BDT) units as central conjugated electron-rich units are promising and widely used donor units in A-D-A type SMDs, which effectively improve the charge transfer and promote the π electron delocalization within molecule. Therefore, the strong π-π interaction between molecules is promoted, which is conducive to the preparation of materials with stronger crystallinity. Typically, Hou's group adopted the single-bond-linked donor strategy and replaced the central donor unit BDT with 3BDT to design and synthesize two donors DRTB-O with alkoxyls and DRTB-T with alkyl-thienyls as side chains. And the authors found that the two donors exhibited different crystalline structures in solid films and after blending with IDIC [37], the PCEs of DRTB-O:IDIC and DRTB-T:IDIC based devices were 0.15% and 9.06% in OSCs, respectively [22]. Subsequently, this group also obtained four donors with 3BDT as the central donor unit, *i.e.*, DRTB-T-C2, DRTB-T-C4, DRTB-T-C6 and DRTB-T-C8, and a top PCE of up to 11.24% is achieved with a DRTB-T-C4:IT-4F-based device [38,39]. All these works proved that the single-bond-linked donor strategy played an important role in designing efficient oligomeric donors and researching scientific problems of OSCs.

The DTBDT unit is a linear five-membered fused-ring aromatic hydrocarbon with a thiophene that was attached to each side of the BDT unit, which makes DTBDT have a longer conjugated backbone and a more effective π electron delocalization than BDT unit, thus achieving stronger intermolecular π-π interactions in donors [40–42]. Recently, our group reported the synthesis of a DTBDT-based SMDs, named ZR1, which produced an excellent PCE of 14.34% with Y6 as acceptor, due to a relatively broader absorption spectrum of small molecule acceptor Y6. Furthermore, the ZR1:Y6 blends performed an optimizing hierarchical morphology due to the high crystallinity of ZR1. In this study, the existence of hierarchical morphologies is important for the charge separation and transport, and ultimately led to a high PCE. Hence, this work provides opportunities to design highly efficient SMDs with DTDBT central donor unit for ASM-OSCs [43]. Subsequently, based on ZR1, our group also designed and synthesized a series of SMDs with DTBDT as donor unit, which showed excellent photovoltaic performance in ASM-OSCs [44–46]. On the basis of these and the relevant studies, we intend to introduce the linked DTBDT to replace DTBDT to design and synthesize corresponding oligomeric donors, which will achieve a larger conjugated plane and a more effective π-π molecular interactions between oligomeric donors and could regulate the molecular stacking orientation and crystallinity of donors and blend films well, so expecting to achieve higher performance in OSCs.

Herein, two novel A-D-D-A type oligomeric donors 2DTBDT and 2DTBDT-2T with linked-DTBDT as central donor unit, without and with bithiophene as the π bridge respectively are designed and synthesized successfully (Fig. 1a). The π bridge provided 2DTBDT-

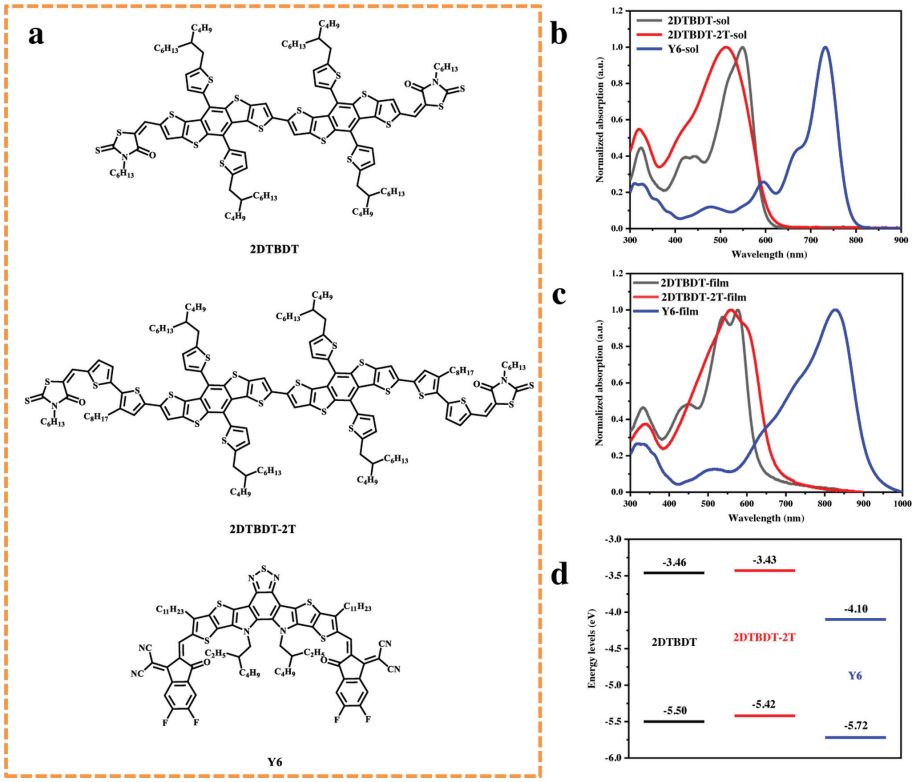

Fig. 1. (a) Molecular structures and UV–vis absorption spectra of oligomeric donors 2DTBDT, 2DTBDT-2T and small molecule acceptor (SMA) Y6 in (b) solution and (c) films and (d) molecular energy-level diagram.

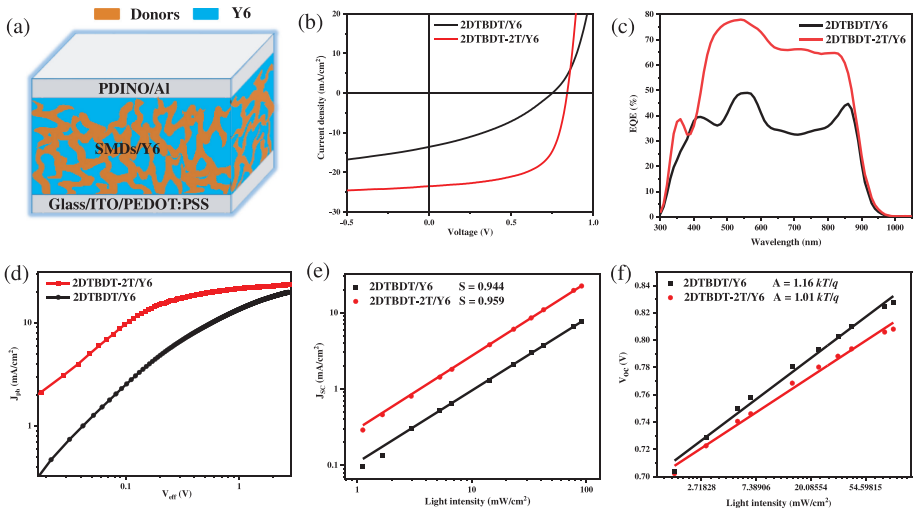

Fig. 2. (a) Schematic illustration of the device structure in this work. (b) *J-V* curves and (c) EQE curves of the optimized 2DTBDT:Y6 and 2DTBDT-2T:Y6 devices. The J_{ph} plotted against the V_{eff} for the (d) optimal OSCs and the corresponding light intensity dependence of (e) J_{SC} and (f) V_{OC}.

Table 1
Detailed photovoltaic parameters of the 2DTBDT and 2DTBDT-2T-based OSCs under simulated air mass (AM) 1.5 G (100 mW/cm^2) illumination.

Donors:Y6	V_{OC} (V)	J_{SC} (mA/cm^2)	FF (%)	PCE (%)
2DTBDT:Y6	0.747 ± 0.014 (0.750)	13.35 ± 0.62 (13.55)	35.09 ± 0.32 (35.71)	3.50 ± 0.25 (3.63)
2DTBDT-2T:Y6	0.838 ± 0.009 (0.840)	24.01 ± 0.46 (23.61)	58.79 ± 1.77 (62.06)	11.83 ± 0.34 (12.31)

Average PCE values were obtained from 10 devices. The parameters based on the best device are shown in parentheses.

2T with 12.31% efficiency and 2DTBDT with merely 3.63% efficiency mixed with Y6 in OSCs. Compared to the 2DTBDT:Y6 blend films, the 2DTBDT-2T:Y6 blend films with nanofiber structure achieved a smoother surface, stronger crystallinity and more uniform phase separation, which delivered more efficient exciton dissociation, reduced biomolecule recombination and higher carrier mobilities in OSCs. Therefore, the 2DTBDT-2T:Y6 devices obtained better fill factor (FF) and PCEs. These findings demonstrate that the single-bond-linked donor strategy combined with π bridge engineering is an alternative method to design the oligomeric donors towards high-performance OSCs.

The synthetic routes of the oligomeric donors 2DTBDT and 2DTBDT-2T are presented in Scheme S1 (Supporting information). And the detailed synthesis methods, ^{1}H nuclear magnetic resonance (^{1}H NMR) and matrix-assisted laser desorption/ionization time of flight mass spectrometry (MALDI-TOF MS) analysis were clearly provided the Supporting information. To explore the optical properties of the oligomeric donors 2DTBDT and 2DTBDT-2T, the UV–vis absorption of donors and acceptor was measured in chloroform solution as well as in thin films, as shown in Figs. 1b and c. In the solution state, 2DTDBT-2T showed wider absorption than 2DTBDT, but no significant shoulder peak appeared, meaning that the two donors did not form the pre-aggregation. However, the absorption curves of two small molecules in thin films showed obvious difference, which suggests that π-π stacking interactions of these molecules were different. Obviously, the 2DTBDT films exhibit the first main peak at 540 nm and a sharp shoulder peak at 578 nm in films, and the 2DTBDT-2T films show the main peak at 560 nm and a gentle shoulder peak at 596 nm in films, which implies that both donors have stronger intermolecular interaction in the films than those in solutions. However, compared with 2DTBDT, the 2DTBDT-2T films performed reduced molecule aggregation and a stronger and wider absorption. Likewise, the absorption edge of 2DTBDT and 2DTBDT-2T films are located at 626 nm and 675 nm, corresponding to the optical bandgap of 1.98 eV and 1.84 eV, respectively. Therefore, the oligomeric donors 2DTBDT and 2DTBDT-2T can both effectively provide complementary absorption for Y6, which is beneficial to achieve high short circuit current density (J_{SC}).

The highest occupied molecular orbitals (HOMO) and lowest unoccupied molecular orbitals (LUMO) of the oligomeric donors 2DTBDT and 2DTBDT-2T in the thin films were determined by obtaining cyclic voltammetry measurements with Ag/Ag$^+$ as the reference electrode (Fig. S1 in Supporting information). The result was shown in Fig. 1d. According to the equation of $E_{HOMO/LUMO} = -(E_{ox/red} - E_{Fc/Fc}{}^{1/2} + 4.8)$ eV [38,47], the HOMO/LUMO of the 2DTBDT and 2DTB- DT-2T were calculated to be –5.50/–3.46 and –5.42/–3.43. Obviously, the identical end-group in the two donors provides similar LUMO levels, whereas the introduction of π bridge enhances the electron donating ability within the 2DTBDT-2T molecule, resulting in a higher HOMO level and a narrower band gap, which is consistent with the UV–vis results. Additionally, the oligomeric donors 2DTBDT and 2DTBDT-2T exhibited appropriate molecular energy level alignment with Y6, which is necessary for the efficient driving force for charge separation.

To investigate the photovoltaic performance, we fabricated OSCs using a conventional architecture of indium tin oxide (ITO)/poly(3,4-ethylenedioxythiophene):polystyrene sulfonate (PEDOT:PSS)/oligomeric donors:Y6/electron transfer layer/Al (Fig. 2a). As shown in the current density-voltage (*J-V*) plots (Fig. 2b) and the summary of the detailed parameters (Table 1), the 2DTBDT:Y6 based devices revealed a V_{OC} of 0.750 V, a J_{SC} of 13.55 mA/cm^2, a FF of 35.71% and ultimately a PCE of 3.63%. However, the 2DTBDT-2T:Y6 devices exhibited enhanced J_{SC} of 23.61 mA/cm^2 and FF of 62.06%, as compared 2DTBDT:Y6, revealed obvious better PCE of 12.31%. Likewise, the external quantum efficiency (EQE) measurements of two optimized systems were carried out to explain the difference in the J_{SC} values of the blended films (Fig. 2c). Even though all the blends exhibited a broad range from 300 nm to 1000 nm, a different EQE response intensity was observed with

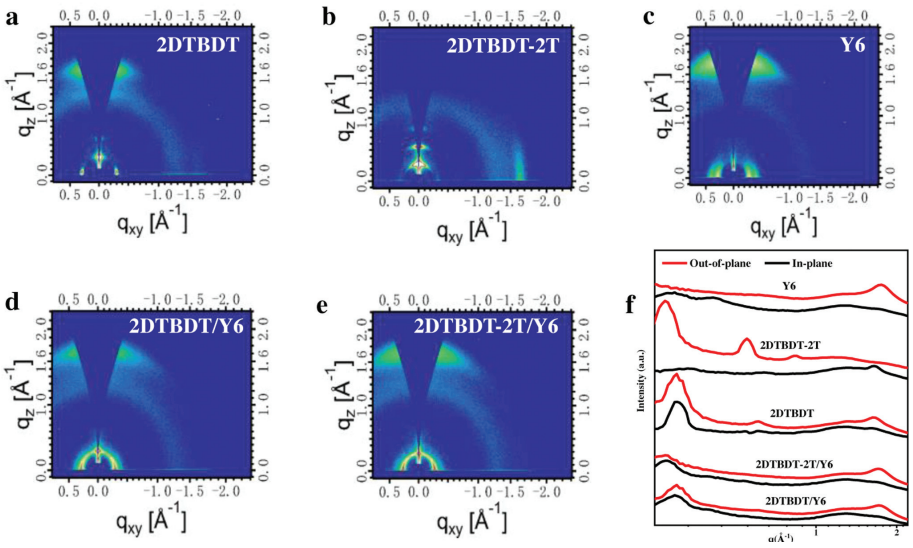

Fig. 3. 2D GIWAXS patterns of (a) 2DTBDT neat films, (b) 2DTBDT-2T neat films, (c) Y6 neat films, (d) 2DTBDT:Y6 blend films and (e) 2DTBDT-2T:Y6 blend films. (f) Corresponding cutline profiles, along with OOP and IP direction.

the maximum value of 49.08% and 77.89% and the integrated J_{SC} values from EQE curves were 13.00 mA/cm^2 and 22.13 mA/cm^2 for 2DTBDT and 2DTBDT-2T based devices, respectively, which is almost in agreement with the results of the *J-V* tests.

Moreover, to understand the exciton dissociation and charge collection characteristics of the 2DTBDT:Y6 and 2DTBDT-2T:Y6 systems in the OSCs, the experiments of comparing the photogenerated current density (J_{ph}) and effective voltage (V_{eff}) were carried out (Fig. 2d). The J_{ph} is the difference between light current density and dark current density, the V_{eff} is the difference value between the compensation voltage (V_0, determined when the J_{ph} is zero) and the applied external voltage bias (V_{app}). The exciton dissociation probability (η_{diss}) was estimated using the equation of $\eta_{diss} = J_{ph}/J_{sat}$, where J_{sat} is the saturation photocurrent density, and charge collection efficiency ($\eta_{cc} = J_{max\ power}/J_{sat}$). Under short circuit conditions, the η_{diss} of 2DTBDT:Y6 and 2DTBDT-2T:Y6 based devices were calculated to be 63.18% and 93.11%, respectively, and the η_{cc} of 2DTBDT:Y6 and 2DTBDT-2T:Y6 based devices were calculated to be 36.65% and 83.71%, respectively, indicating that the 2DTBDT-2T:Y6 based device has a higher efficiency in the photogenerated exciton dissociation and charge collection.

Furthermore, we carried out the incident light intensity (*P*) dependent *J-V* characterization to investigate the different charge recombination of two systems in the devices. The relationship between J_{SC} and *P* can be quantitatively interpreted using a power-law function in which the parameter is close to unity when the bimolecular recombination is negligible (Fig. 2e). The estimated values are 0.944 and 0.959 for the 2DTBDT:Y6 and 2DTBDT-2T:Y6 devices, respectively, implying the reduced bimolecular recombination loss in 2DTBDT-2T:Y6 blend films. The relationship between V_{OC} and *P* was plotted in Fig. 2f. The slopes (A) of these devices are 1.16 kT/q and 1.01 kT/q for the 2DTBDT and 2DTBDT-2T-based devices (k is Boltzmann constant, T is the temperature in Kelvin, and q is the elementary charge), suggesting that the 2DTBDT-2T-based OSCs suppresses trap-assisted recombination, which is beneficial for higher J_{SC} and FF in their corresponding devices.

To directly evaluate the vertical charge carrier mobility of both blend films, the space charge limited current (SCLC) method was used with the hole only device (ITO/PEDOT:PSS/Active layer/MoOx/Ag) and electron only device (ITO/ZnO/Active layer/Ca/Al). We found that 2DTBDT:Y6 had hole and electron mobilities of 5.30×10^{-4} cm^2 V^{-1} s^{-1} and 1.20×10^{-4} cm^2 V^{-1} s^{-1}, respectively, with a high μ_h/μ_e ratio of 4.42. Such extremely unbalanced charge transport could lead to a severe charge recombination for the corresponding OSCs. By contrast, 2DTBDT-2T:Y6 not only afforded increased hole and electron mobilities of 5.61×10^{-4} cm^2 V^{-1} s^{-1} and 2.46×10^{-4} cm^2 V^{-1} s^{-1}, respectively, but also had a more balanced μ_h/μ_e ratio of 2.28, which can partly explain its improved J_{SC} and FF values as well as PCE values for the 2DTBDT-2T:Y6 than 2DTBDT:Y6 devices in OSCs.

To deeply understand the difference in photovoltaic performances of the 2DTBDT:Y6 and 2DTBDT-2T:Y6, grazing incidence wide-angle X-ray scattering (GIWAXS) measurements were performed to analyze crystallinity and molecular stacking orientation of both neat oligomeric donors and their blend films. The 2D GIWAXS patterns and corresponding cutline profiles in the in-plane (IP) and out-of-plane (OOP) directions are shown in Figs. 3a-f. The acceptor Y6 shows a clear and strong face-on orientation, and the neat film 2DTBDT performs the predominant face-on orientation resulting from strong π-π (010) diffraction peaks in the OOP direction and lamella stacking (100) peaks in the IP direction. In contrast, the neat films 2DTBDT-2T exhibit the π-π (010) diffraction peaks in the IP direction and lamella stacking (100), (200) and (300) peaks in the OOP direction, which indicates that it has a preferential edge-on orientation. Similar to the traditional A-D-A type SMAs, we speculated that when the central D unit was directly connected to end-group, intermolecular stacking tended to assemble *via* the end-group π–π stacking at the liquid–vapor interfaces during solvent evaporation, which is beneficial to enhance horizontal and face-on orientations. However, the oligomeric donor 2DTBDT-2T with a π bridge has a longer conjugated structure and a greater configurational twist, which makes molecules prone to stacking between conjugated units and reduced end-group stacking during film formation, resulting in an edge-on orientation relative to the substrate (Fig. S2 in Supporting information). After blending with Y6, both films exhibit the face-on arrangement, which is beneficial for the charge transport in OSCs towards the electrodes. However, compared with 2DTBDT:Y6 films ($q = 1.72$ Å, $d = 3.67$ nm, CCL = 14.79 nm), the 2DTBDT-2T:Y6 films in the OOP direction show similar π-π interactions distance and longer crystal coherent length (CCL) ($q = 1.71$ Å, $d = 3.67$ nm, CCL = 18.34 nm), which indicate that the 2DTBDT-2T:Y6 films can obtain stronger crystallinity and better vertical charge transport, which is conducive to form more suitable phase separation scale. Compared

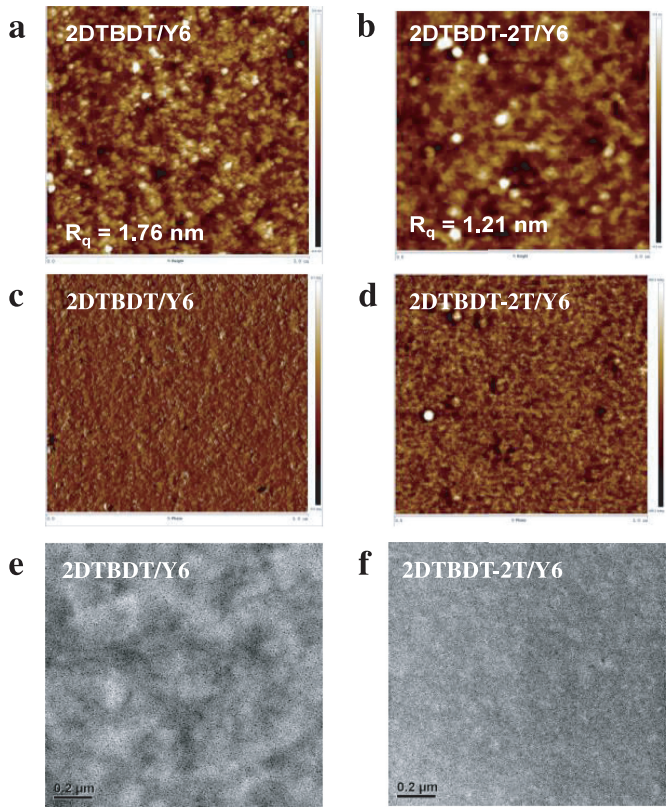

Fig. 4. AFM height, phase and TEM images of (a, c, e) 2DTBDT:Y6 film and (b, d, f) 2DTBDT-2T:Y6 film.

with oligomeric donor 2DTBDT:Y6, the molecular stacking orientation of oligomeric donor 2DTBDT-2T was completely different from that of Y6, and the donor was induced to face-on orientation by the acceptor during the process of the film formation, which also enhanced the crystallinity of the blend film.

The surface morphology of the blend films was also investigated by atomic force microscopy (AFM) and transmission electron microscopy (TEM) as shown in Fig. 4. The AFM height images show that the optimized 2DTBDT-2T:Y6 film exhibits a mean-square surface roughness (R_q) of 1.21 nm and the optimized 2DTBDT:Y6 film is 1.76 nm, which indicates a smoother surface of optimized 2DTBDT-2T:Y6 film (Figs. 4a and b). Simultaneously, the phase images show that 2DTBDT:Y6 film shows large-scale phase separation and 2DTBDT-2T:Y6 film performs an obvious nano-scale bicontinuous interpenetrating network with clear phase separation, (Figs. 4c and d). Similarly, in the TEM images (Figs. 4e and f), the blend film 2DTBDT:Y6 shows a large phase domain and phase separation scale, which is not conducive to exciton dissociation in active layers. On the contrary, 2DTBDT-2T:Y6 performs a small phase separation scale and obvious nanofiber structure, which is consistent with the results from AFM images and directly related to the higher J_{SC} and FF in their corresponding devices.

In summary, we designed and synthesized two A-D-D-A type oligomeric donors 2DTBDT and 2DTBDT-2T with single-bond-linked DTBDT as donor units, without and with bithiophene as the π bridge, respectively. We found that the neat film 2DTBDT performed the predominant face-on orientation, whereas the neat film 2DTBDT-2T had a preferential edge-on orientation. And the π bridge engineering provided 2DTBDT-2T with 12.31% PCE, 23.61 mA/cm^2 J_{SC} and 62.06% FF, and 2DTBDT with merely 3.63% PCE, 13.55 mA/cm^2 J_{SC} and 35.71% FF, mixed with Y6 in OSCs, which is mainly due to the stronger and wider absorption spectrum of the former. In addition, compared to 2DTBDT:Y6 blend films, the 2DTBDT-2T:Y6 blend films with nanofiber structure achieved a smoother surface, stronger crystallinity and more uniform phase separation, which delivered more efficient exciton dissociation and collection, reduced biomolecule recombination and higher and more balanced carrier mobilities in their OSCs. Therefore, the 2DTBDT-2T:Y6 devices obtained better FF and PCEs. These findings demonstrate that the single-bond-linked donor strategy combined with π bridge engineering is an alternative method to design the donors towards high-performance OSCs.

Declaration of competing interest

The authors declare that they have no known competing financial interests or personal relationships that could have appeared to influence the work reported in this paper.

Acknowledgments

We acknowledge financial support provided by the National Natural Science Foundation of China (Nos. 21822503 and 51973043), and the Youth Innovation Promotion Association, the Chinese Academy of Sciences (No. GJHZ2092-019).

Supplementary materials

Supplementary material associated with this article can be found, in the online version, at doi:10.1016/j.cclet.2022.03.044.

References

[1] M. Kaltenbrunner, M.S. White, E.D. Glowacki, et al., Nat. Commun. 3 (2012) 770.
[2] C.J. Brabec, M. Heeney, I. McCulloch, J. Nelson, Chem. Soc. Rev. 40 (2011) 1185–1199.
[3] S.D. Collins, N.A. Ran, M.C. Heiber, T.Q. Nguyen, Adv. Energy Mater. 7 (2017) 1602242.
[4] R.Z. Liang, M. Babics, A. Seitkhan, et al., Adv. Funct. Mater. 28 (2018) 1705464.
[5] O. Inganas, Adv. Mater. 30 (2018) 1800388.
[6] D.Q. Hu, H. Tang, J. Lv, et al., Sustain. Energ. Fuels 5 (2021) 3593–3597.
[7] C.B. An, Y.P. Qin, T. Zhang, et al., J. Mater. Chem. A 9 (2021) 13653–13660.
[8] Q.L. Lv, C.B. An, T. Zhang, et al., Sci. China Chem. 64 (2021) 1200–1207.
[9] M. Lv, R.M. Zhou, K. Lu, Z.X. Wei, Acta Chim. Sin. 79 (2021) 284–302.
[10] C. Yang, M. Lv, R.M. Zhou, et al., Adv. Energy Sustain. Res. 2 (2021) 2100099.
[11] J. Yuan, Y.Q. Zhang, L.Y. Zhou, et al., Joule 3 (2019) 1140–1151.
[12] T. Jia, J.B. Zhang, W.K. Zhong, et al., Nano Energy 72 (2020) 104718.
[13] J.Y. Wu, J. Lee, Y.C. Chin, et al., Energy Environ. Sci. 13 (2020) 2422–2430.
[14] S.S. Chen, J.F. Ye, Q.G. Yang, et al., J. Mater. Chem. A 9 (2021) 2857–2863.
[15] Y. Cui, Y. Xu, H.F. Yao, et al., Adv. Mater. 33 (2021) 2102420.
[16] J.Z. Qin, Z.H. Chen, P.Q. Bi, et al., Energy Environ. Sci. 14 (2021) 5903–5910.
[17] B. Kan, Y.Y. Kan, L.J. Zuo, et al., InfoMat 3 (2021) 175–200.
[18] W.Y. Ye, Y. Yang, Z.Z. Zhang, et al., Sol. RRL 4 (2020) 2000258.
[19] C. He, J.H. Hou, Acta Phys. Chim. Sin. 34 (2018) 1202–1210.
[20] Z.C. Zhou, S.J. Xu, J.N. Song, et al., Nat. Energy 3 (2018) 952–959.
[21] X.X. Dai, X.D. Cheng, Z.P. Kan, et al., Chin. J. Org. Chem. 40 (2020) 4031–4045.
[22] S.Q. Zhang, L.Y. Yang, D.L. Liu, et al., Sci. China Chem. 60 (2017) 1340–1348.
[23] X.F. Cheng, M.M. Li, Z.Q. Guo, et al., J. Mater. Chem. A 7 (2019) 23008–23018.
[24] H. Li, J. Fang, J.Q. Zhang, et al., Mat. Chem. Front. 2 (2018) 143–148.
[25] H. Li, Q. Wu, R.M. Zhou, et al., Adv. Energy Mater. 9 (2019) 1803175.
[26] D.B. Yang, K.B. Yu, J. Xu, et al., J. Mater. Chem. A 9 (2021) 10427–10436.
[27] X.F. Cheng, M.M. Li, Z.Q. Liang, et al., ACS Appl. Energ. Mater. 4 (2021) 8442–8453.
[28] Q. ul Ain, R.A. Shehzad, U. Yaqoob, et al., Comput. Theor. Chem. 1200 (2021) 113238.
[29] X.C. Wang, D. Huang, J.H. Han, et al., ACS Appl. Mater. Interfaces 13 (2021) 11108–11116.
[30] X.Y. Dong, D.Q. Hu, P.Y. Chen, et al., J. Semicond. 41 (2020) 1674–4926.
[31] M. Khalid, R.A. Khera, S. Jabeen, P. Langer, J. Iqbal, Comput. Theor. Chem. 1183 (2020) 112848.
[32] S.M. Li, Q. Ma, B.B. Qiu, et al., Sol. RRL 5 (2021) 2100515.
[33] X.C. Wang, J.H. Han, H.X. Jiang, et al., ACS Appl. Mater. Interfaces 11 (2019) 44501–44512.
[34] W.Y. Liu, Z.C. Zhou, T. Vergote, S.J. Xu, X.Z. Zhu, Mat. Chem. Front. 1 (2017) 2349–2355.
[35] Y.R. Cheon, Y.J. Kim, J.Y. Back, et al., J. Mater. Chem. A 2 (2014) 16443–16451.
[36] J. Guo, H.J. Bin, W. Wang, et al., J. Mater. Chem. A 6 (2018) 15675–15683.
[37] Y.Z. Lin, Q. He, F.W. Zhao, et al., J. Am. Chem. Soc. 138 (2016) 2973–2976.
[38] L.Y. Yang, S.Q. Zhang, C. He, et al., Chem. Mat. 30 (2018) 2129–2134.

[39] W.C. Zhao, S.S. Li, H.F. Yao, et al., J. Am. Chem. Soc. 139 (2017) 7148–7151.
[40] Y. Wu, Z.J. Li, X. Guo, et al., J. Mater. Chem. 22 (2012) 21362–21365.
[41] M. Jung, D. Seo, K. Kwak, et al., Dyes Pigm. 115 (2015) 23–34.
[42] H.I. Je, J. Hong, H.J. Kwon, et al., Dyes Pigm. 157 (2018) 93–100.
[43] R.M. Zhou, Z.Y. Jiang, C. Yang, et al., Nat. Commun. 10 (2019) 5393.
[44] R.M. Zhou, C. Yang, W.J. Zou, et al., J. Energy Chem. 52 (2021) 228–233.
[45] R.M. Zhou, Z.Y. Jiang, Y.A. Shi, et al., Adv. Funct. Mater. 30 (2020) 2005426.
[46] Z.Y. Huang, R.M. Zhou, M. Lv, et al., Mat. Chem. Front. 5 (2021) 1405–1409.
[47] Y. Qin, Y.L. Chang, X.W. Zhu, et al., Nano Today 41 (2021) 101289.